THE INFLUENCE OF REACTIVE TORQUES ON COMET NUCLEUS ROTATION

A. I. NEISHTADT[1], D. J. SCHEERES[2], V. V. SIDORENKO[3,*], P. J. STOOKE[4] and A. A. VASILIEV[1]
[1]*Space Research Institute, Moscow, Russia*
[2]*Department of Aerospace Engineering, The University of Michigan, Ann Arbor, MI, U.S.A.*
[3]*Keldysh Institute of Applied Mathematics, Miusskaya Sq. 4, 125047, Moscow, Russia*
[4]*Department of Geography, The University of Western Ontario, London, Ont, Canada*

(Received: 29 March 2002; revised: 7 October 2002; accepted: 18 November 2002)

Abstract. Reactive torques, due to anisotropic sublimation on a comet nucleus surface, produce slow variations of its rotation. In this paper the secular effects of this sublimation are studied. The general rotational equations of motion are averaged over unperturbed fast rotation around the mass center (Euler-Poinsot motion) and over the orbital comet motion. We discuss the parameters that define typical properties of the rotational evolution and discover different classifications of the rotational evolution. As an example we discuss some possible scenarios of rotational evolution for the nuclei of the comets Halley and Borrelly.

Key words: comet nucleus, rotational dynamics, non-gravitational perturbations

1. Statement of the Problem and Main Assumptions

In the classical model of a comet nucleus proposed by Whipple (1951), anisotropic ice sublimation due to solar radiation produces reactive torques, $\mathbf{M}^{\mathrm{r}}$, that act on the nucleus. The goal of the present paper is to study the possible secular effects produced by $\mathbf{M}^{\mathrm{r}}$ on the rotational dynamics of the nucleus. Unlike previous studies, based primarily on numerical modeling of nucleus rotation evolution (Wilhelm, 1987; Peale and Lissauer, 1989; Julian, 1990; Samarasinha and Belton, 1995; Szegö et al., 2001; Jorda and Licandro, in Press), we use an averaging method (Bogolyubov and Mitropolsky, 1961; Arnold, 1978) to extract the secular components of the nucleus motion.

We approximate the nucleus surface by a polyhedron with an arbitrary number of faces. As an example, Figure 1 shows such an approximation for the comet Halley nucleus. The shape of this nucleus is reconstructed on the basis of TV images obtained by the missions 'Vega-1,2' and 'Giotto' (Stooke and Abergel, 1991, unpublished).

*Author for correspondence: Tel.: +7-0952507876; Fax: +7-0959720737; e-mail: sidorenk@spp.keldysh.ru

List of symbols is given in the Appendix.

Celestial Mechanics and Dynamical Astronomy **86:** 249–275, 2003.

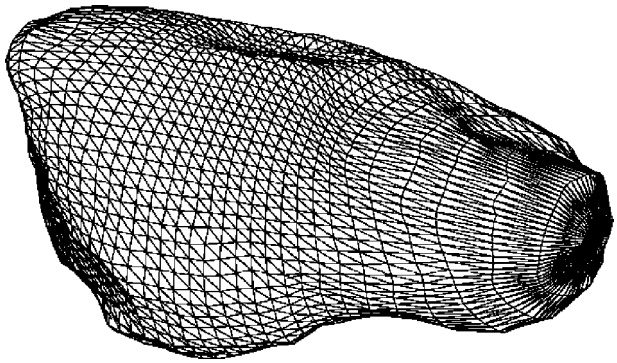

Figure 1. P/Halley nucleus: reconstruction based on Vega-1,2 and Giotto images.

Reactive torques due to ice sublimation can be evaluated with the use of the approximate formula:

$$\mathbf{M}^{\mathrm{r}} = -\sum_{j=1}^{N} Q_j(\mathbf{R}_j \times \mathbf{v}_j), \tag{1}$$

where N is the number of faces of the approximating polyhedron, Q_j is the mass ejection rate on the jth face, $\mathbf{R}_j$ is the radius vector of the face's center in the body principal frame of reference, and $\mathbf{v}_j$ is the effective velocity of the ejected matter.

The mass ejection rate depends on local illumination conditions and the heliocentric distance, and is difficult to describe accurately (Crifo and Rodionov, 1999). Following Peale and Lissauer (1989), Julian (1990), Samarasinha and Belton (1995), in this paper we use an empirical expression to calculate Q_j

$$Q_j = s_j g(r) f(\delta_j) Q_*. \tag{2}$$

Here Q_* is the mass ejection rate from a plane surface of area equal to the total surface area of the nucleus, oriented perpendicular to the Sun line of sight at a heliocentric distance of 1 AU, s_j is the relative intensity (the ratio of the maximal possible mass ejection rate from the jth face at this heliocentric distance to Q_*), δ_j is the angle between the outer normal to the face $\mathbf{n}_j$ and the unit vector pointing to the Sun $\mathbf{e}_{\mathrm{S}}$, and r is the heliocentric distance.

The function $g(r)$ describes the dependence of the mass ejection rate on the heliocentric distance. It is given by the expression (Marsden et al., 1973):

$$g(r) = g_0\left(\frac{r}{r_0}\right)^{-c_1}\left[1 + \left(\frac{r}{r_0}\right)^{c_2}\right]^{-c_3}, \tag{3}$$

where

$$c_1 = 2.15, \quad c_2 = 5.093, \quad c_3 = 4.6142, \quad r_0 = 2.808, \quad g_0 = 0.111262.$$

The function $f(\delta_j)$ defines the dependence of the mass ejection rate on the angle between the direction to the Sun and the normal to the jth face. Following Weeks (1995), we assume that

$$f(\delta_j) = 1 - \alpha(1 - \cos\delta_j). \tag{4}$$

The coefficient α in Equation (4) can be chosen to be 1/2 or slightly less. Small variations of its value do not substantially affect the properties of nucleus motion under the scope of our model (Sections 2 and 3). When it is necessary to apply numeric methods (for example, to compare different variants of the nucleus motion evolution in Section 2) we use $\alpha = 1/2$ since there are no serious reasons to prefer any another value of this coefficient.

We consider reactive torques as the only factor changing the nucleus rotation state; thus, we neglect variations in the nucleus shape and its moments of inertia due to matter sublimation. In addition, we neglect energy dissipation due to non-stationary deformations of the rotating nucleus caused by inertia forces. This approach is quite traditional in studies of spin evolution of short-period comets on time periods several tens or hundreds of orbits around the Sun (Samarasinha and Belton, 1995). We also assume that the comet orbit, defined by eccentricity e and perihelion distance q, does not change (in the future we plan to study the influence of the orbit evolution on the evolution of the rotational state).

2. Equations of Motion

To describe the rotation of the comet nucleus, we introduce three right-hand orthogonal coordinate systems with their origin at the center of mass of the nucleus (Figure 2):

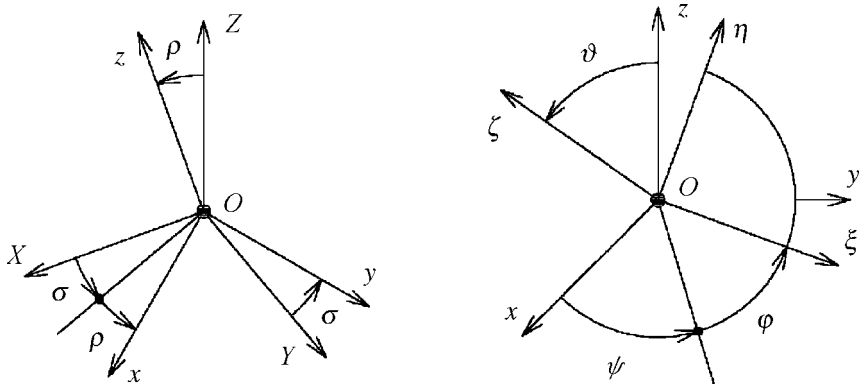

Figure 2. Angles and coordinate systems used to describe the comet nucleus motion.

OXYZ: The 'perihelion' system, with the *OZ*-axis parallel to the Sun–perihelion line, the *OY*-axis normal to the plane of the orbit, and the *OX*-axis parallel to the tangent to the orbit at perihelion and directed along the orbit motion. As we assume that the orbit is not evolving, the 'perihelion' coordinate system has a permanent orientation in absolute space.

Oxyz: The frame connected with the angular momentum vector of the nucleus **L**. The *Oz* axis is directed along **L**, the *Oy* axis is in the plane *OXY*.

$O\xi\eta\zeta$: The body-fixed system, the axes $O\xi$, $O\eta$, $O\zeta$ being the principal inertia axes. The moments of inertia of the nucleus with respect to these axes are defined as A_*, B_*, C_* respectively, and satisfy the condition

$$A_* > B_* > C_*.$$

We define the orientation of the coordinate system *Oxyz* with respect to the 'perihelion' system *OXYZ* with the use of the angles ρ and σ (Figure 2). A turn through the angle σ around the *OZ* axis followed by a turn through the angle ρ around the *Oy* axis puts the trihedron *Oxyz* into its current position from an initial position coinciding with the trihedron *OXYZ*. The corresponding transfer matrix has the form:

	x	y	z
X	m_{Xx}	m_{Xy}	m_{Xz}
Y	m_{Yx}	m_{Yy}	m_{Yz}
Z	m_{Zx}	m_{Zy}	m_{Zz}

$$\begin{aligned} m_{Xx} &= \cos\sigma\cos\rho, \quad m_{Yx} = \sin\sigma\cos\rho, \quad m_{Zx} = -\sin\rho, \\ m_{Xy} &= -\sin\sigma, \quad m_{Yy} = \cos\sigma, \quad m_{Zy} = 0, \\ m_{Xz} &= \cos\sigma\sin\rho, \quad m_{Yz} = \sin\sigma\sin\rho, \quad m_{Zz} = \cos\rho. \end{aligned}$$

We define the orientation of the system $O\xi\eta\zeta$ with respect to the system *Oxyz* by the Euler angles φ, ϑ, ψ. The transfer matrix is

	ξ	η	ζ
x	$a_{x\xi}$	$a_{x\eta}$	$a_{x\zeta}$
y	$a_{y\xi}$	$a_{y\eta}$	$a_{y\zeta}$
z	$a_{z\xi}$	$a_{z\eta}$	$a_{z\zeta}$

$$\begin{aligned} a_{x\xi} &= \cos\varphi\cos\psi - \sin\varphi\sin\psi\cos\vartheta, \\ a_{y\xi} &= \sin\varphi\cos\psi + \cos\varphi\sin\psi\cos\vartheta, \quad a_{z\xi} = \sin\psi\sin\vartheta, \\ a_{x\eta} &= -\cos\varphi\sin\psi - \sin\varphi\cos\psi\cos\vartheta, \end{aligned}$$

$$a_{y\eta} = -\sin\varphi\sin\psi + \cos\varphi\cos\psi\cos\vartheta, \quad a_{z\eta} = \sin\vartheta\cos\psi,$$
$$a_{x\zeta} = \sin\vartheta\sin\varphi, \quad a_{y\zeta} = -\sin\vartheta\cos\varphi, \quad a_{z\zeta} = \cos\vartheta.$$

The complete set of equations of the comet nucleus motion consists of the equations describing its rotation in the coordinate system $Oxyz$ and the equations for the time evolution of its angular momentum vector.

It is convenient to use dimensionless variables and parameters in the equations of motion. Take as an independent variable $\tau = \Omega_* t$, where Ω_* is the initial angular velocity of the nucleus. The dimensionless variable L is the ratio of the magnitude of the angular momentum vector to $L_* = I_*\Omega_*$ (here $I_* = m_* R_*^2$, m_* is the nucleus mass, and R_* is its typical linear size). Then the parameters A, B, C are the dimensionless moments of inertia:

$$A = \frac{A_*}{I_*}, \quad B = \frac{B_*}{I_*}, \quad C = \frac{C_*}{I_*}.$$

For example, if the nucleus shown in Figure 1 is homogeneous and $R_* = 5$ km is taken as its typical linear size, we have

$$A = 0.6121, \quad B = 0.5857, \quad C = 0.2129.$$

Relations for moments of inertia of celestial bodies of irregular shape approximated by polyhedrons are given by Dobrovolskis (1996).

Taking into account the assumptions made above, we can write the equations of motion in the following form (Beletskii, 1966):

$$\begin{aligned}
\frac{\mathrm{d}\vartheta}{\mathrm{d}\tau} &= L\sin\vartheta\sin\psi\cos\psi\left(\frac{1}{A} - \frac{1}{B}\right) + \\
&\quad + \frac{1}{L}[(M_\xi^{\mathrm{r}}\sin\psi + M_\eta^{\mathrm{r}}\cos\psi)\cos\vartheta - M_\zeta^{\mathrm{r}}\sin\vartheta], \\
\frac{\mathrm{d}\varphi}{\mathrm{d}\tau} &= L\left(\frac{\sin^2\psi}{A} + \frac{\cos^2\psi}{B}\right) - \frac{M_x^{\mathrm{r}}}{L}\cos\varphi\,\mathrm{ctg}\,\vartheta - \\
&\quad - \frac{M_y^{\mathrm{r}}}{L}(\mathrm{ctg}\,\rho + \sin\varphi\,\mathrm{ctg}\,\vartheta), \\
\frac{\mathrm{d}\psi}{\mathrm{d}\tau} &= L\cos\vartheta\left(\frac{1}{C} - \frac{\sin^2\psi}{A} - \frac{\cos^2\psi}{B}\right) + \frac{M_\xi^{\mathrm{r}}\cos\psi - M_\eta^{\mathrm{r}}\sin\psi}{L\sin\vartheta},
\end{aligned}$$

TABLE I

Typical parameter values derived from published data (Kamél, 1991; Jorda and Licandro, in Press)

Comet name	Q_* [kg h^{-1}]	R_* [km]	$m_* \cdot 10^{-12}$ [kg]	$I_* \cdot 10^{-12}$ [kg km^2]	Ω_* [h r^{-1}]	ε
Jupiter family comets						
2P/Encke	$5.1 \cdot 10^7$	2.3	53.7	294	0.97	$3.9 \cdot 10^{-4}$
46P/Wirtanen	$3.4 \cdot 10^6$	0.6	0.9	0.32	1	$5.7 \cdot 10^{-3}$
9P/Tempel 1	$5.1 \cdot 10^7$	2.3	53.7	380	0.15	$1.2 \cdot 10^{-2}$
19P/Borrelly	$1.5 \cdot 10^8$	4	85	1360	0.25	$6.4 \cdot 10^{-3}$
Halley-like comets						
1P/Halley	$2.3 \cdot 10^8$	5	525	13100	0.1	$7.9 \cdot 10^{-3}$
109P/Swift-Tuttle	$1.3 \cdot 10^9$	12	7240	10^6	0.1	$1.4 \cdot 10^{-3}$

Note: Estimation of 9P/Tempel 1 nucleus angular velocity is according to private communication by M.J.S. Belton.

$$\frac{\mathrm{d}\rho}{\mathrm{d}\tau} = \frac{M_x^{\mathrm{r}}}{L}, \qquad \frac{\mathrm{d}\sigma}{\mathrm{d}\tau} = \frac{M_y^{\mathrm{r}}}{L\sin\rho}, \qquad \frac{\mathrm{d}L}{\mathrm{d}\tau} = M_z^{\mathrm{r}}. \tag{5}$$

The values M_x^{r}, M_y^{r}, M_z^{r} and M_ξ^{r}, M_η^{r}, M_ζ^{r} in Equations (5) are the projections of the reactive torque onto the corresponding axes of the coordinate systems $Oxyz$ and $O\xi\eta\zeta$:

$$M_x^{\mathrm{r}} = a_{x\xi}M_\xi^{\mathrm{r}} + a_{x\eta}M_\eta^{\mathrm{r}} + a_{x\zeta}M_\zeta^{\mathrm{r}},$$

and similarly for M_y^{r} and M_z^{r} with

$$M_\xi^{\mathrm{r}} = \varepsilon g(r)\sum_{j=1}^{N} s_j d_{j\xi}[(1-\alpha) + \alpha(\mathbf{e}_{\mathrm{S}}, \mathbf{n}_j)],$$

and similarly for M_η^{r} and M_ζ^{r}, where

$$\begin{pmatrix} d_{j\xi} \\ d_{j\eta} \\ d_{j\zeta} \end{pmatrix} = \mathbf{n}_j \times \left(\frac{\mathbf{R}_j}{R_*}\right), \quad \varepsilon = \frac{v_* Q_* R_*}{I_* \Omega_*^2}.$$

Here v_* is the effective velocity of ejected matter.

The parameter ε determines the influence of the reactive torque on the nucleus rotation. Considering ε as a small parameter (in this case the motion is a weakly perturbed Euler-Poinsot motion), we use the averaging method to develop a qualitative description of the solutions of (5). The adequacy of the assumption $\varepsilon \ll 1$ is confirmed for several short-period comets (Table I).

Note an important property of the system (5): if

$$(\vartheta(\tau), \rho(\tau), \sigma(\tau), L(\tau), \psi(\tau), \varphi(\tau))$$

is its solution, then

$$(\pi - \vartheta(-\tau), \pi - \rho(-\tau), \pi + \sigma(-\tau), L(-\tau), \pi + \psi(-\tau), \pi - \varphi(-\tau))$$

is also its solution. This 'reversibility' of solutions is due to the absence of dissipation in the model of forces determining the comet nucleus dynamics.

3. Averaging Approximation

3.1. UNPERTURBED MOTION

To successfully apply the averaging method and interpret the results one should take into consideration the following properties of the unperturbed motion.

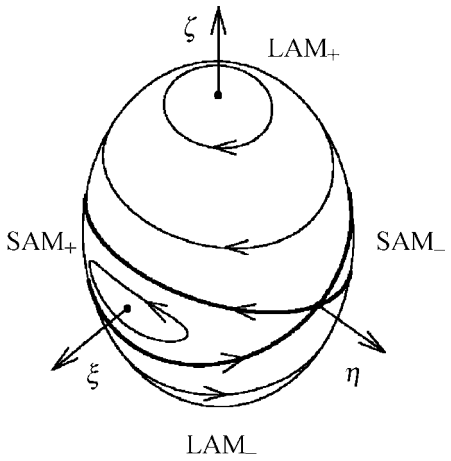

Figure 3. The inertia ellipsoid and polhodes.

At $\varepsilon = 0$ Equations (5) describe the Euler-Poinsot case of a rigid body motion. In that case variables L, σ, ρ are independent of τ and the behavior of variables φ, ϑ, ψ can be described in terms of the Jacobi elliptic functions (Landau and Lifshitz, 1976). The nucleus' inertia ellipsoid rolls without slipping on a fixed plane Π perpendicular to the constant vector of angular momentum $\mathbf{L}$. Points of the inertia ellipsoid that are tangent to the plane Π at different times form a closed curve (polhode). Depending on initial conditions, this curve encircles either $O\xi$ or $O\zeta$ axis (Figure 3).

One can use the following first integral of system (5) for $\varepsilon = 0$ to define the polhode on the inertia ellipsoid:

$$w = \frac{2BT}{L^2} = \left[1 - \left(1 - \frac{1}{\theta_A}\right)\sin^2\psi\right]\sin^2\vartheta + \frac{\cos^2\vartheta}{\theta_C},$$

where T is the kinetic energy of the nucleus rotational motion,

$$\theta_A = \frac{A}{B}, \quad \theta_C = \frac{C}{B}.$$

If $w \in (1/\theta_A, 1)$, the motion is called a complex short axis mode (complex SAM): the polhodes encircle the shortest axis of the inertia ellipsoid $O\xi$. If $w \in (1, 1/\theta_C)$, the motion is called a complex long axis mode (complex LAM): the polhodes encircle the longest axis of the inertia ellipsoid $O\zeta$. At $w = 1/\theta_A$ the polhodes degenerate into points, corresponding to rotation around the axis with the largest inertia momentum (simple SAM). Similarly $w = 1/\theta_C$ corresponds to rotation around the axis with the smallest inertia momentum (simple LAM). Note, these classifications of motion are not usual and cannot be found in classic monographs on rigid body dynamics. Nevertheless, they are often used in studies of the rotation of celestial bodies (see, for example, Kinoshita (1992), Samarasinha and Belton (1995)).

If $w = 1$, the motion is asymptotic: as $\tau \to \pm\infty$ the immediate rotation axis tends to the $O\eta$ axis. The polhodes corresponding to the asymptotic motions are separatrices separating polhodes of complex SAM and complex LAM (Figure 3).

SAMs (complex and simple) can be divided into subsets SAM_+ and SAM_- where the projection of the angular velocity vector $\mathbf{\Omega}$ onto the axis $O\xi$ is correspondingly positive or negative. In the same way LAMs are divided into subsets LAM_+ and LAM_- with different signs of projection of $\mathbf{\Omega}$ onto $O\zeta$ axis.

3.2. CONSTRUCTION OF EVOLUTIONARY EQUATIONS

The evolutionary equations are the closed set of equations for the secular components of variation in the variables σ, ρ, L and the value of w, which varies at $\varepsilon \neq 0$ in accordance with

$$\begin{aligned}\frac{\mathrm{d}w}{\mathrm{d}\tau} &= \frac{2(\mathbf{\Omega}, \mathbf{M}^{\mathrm{r}})}{L^2} - \frac{2w}{L}\frac{\mathrm{d}L}{\mathrm{d}\tau} \\ &= \frac{2}{L}\left[\left(\frac{1}{\theta_A} - w\right)a_{z\xi}M_\xi^{\mathrm{r}} + (1-w)a_{z\eta}M_\eta^{\mathrm{r}} + \left(\frac{1}{\theta_C} - w\right)a_{z\zeta}M_\zeta^{\mathrm{r}}\right].\end{aligned}$$

In the following, w is used as a variable for describing motion of the nucleus with respect to the angular momentum vector.

We construct the evolutionary equations in two steps. First, the right-hand sides of the equations for $\mathrm{d}w/\mathrm{d}\tau$, $\mathrm{d}\sigma/\mathrm{d}\tau$, $\mathrm{d}\rho/\mathrm{d}\tau$, $\mathrm{dL}/\mathrm{d}\tau$ are averaged along the unperturbed motion (Euler-Poinsot motion). SAMs and LAMs are described by different formulae and thus need to be considered separately (however, after a change of notation the expressions for SAMs and LAMs are similar). The second step is to average the equations over the orbital motion.

3.3. EVOLUTIONARY EQUATIONS IN THE FIRST APPROXIMATION OF THE AVERAGING METHOD

Omitting tedious calculations, we present the evolutionary equations obtained:

$$\begin{aligned}\frac{\mathrm{d}w}{\mathrm{d}\tau} &= \frac{2\varepsilon}{L}\left\{(1-\alpha)\Phi_0\left[D_0^\xi\langle a_{z\xi}\rangle_e\left(\frac{1}{\theta_A} - w\right) + D_0^\zeta\langle a_{z\zeta}\rangle_e\left(\frac{1}{\theta_C} - w\right)\right] - \right. \\ &\quad - \alpha\cos\rho\,\Phi_1\left[D_1^\xi\left(\left(\frac{1}{\theta_A} - w\right)\langle a_{z\xi}^2\rangle_e - (1-w)\langle a_{z\eta}^2\rangle_e\right) + \right. \\ &\quad \left.\left. + D_1^\zeta\left(\left(\frac{1}{\theta_C} - w\right)\langle a_{z\zeta}^2\rangle_e - (1-w)\langle a_{z\eta}^2\rangle_e\right)\right]\right\},\end{aligned}$$

$$
\begin{aligned}
\frac{\mathrm{d}\rho}{\mathrm{d}\tau} &= -\frac{\varepsilon\alpha\sin\rho\Phi_1}{2L}\Big[D_1^{\xi}(\langle a_{z\xi}^2\rangle_e - \langle a_{z\eta}^2\rangle_e) + D_1^{\zeta}(\langle a_{z\zeta}^2\rangle_e - \langle a_{z\eta}^2\rangle_e)\Big],\\
\frac{\mathrm{d}\sigma}{\mathrm{d}\tau} &= \frac{\varepsilon\alpha\Phi_1}{2L}(D_2^{\xi}\langle a_{z\xi}\rangle_e + D_2^{\zeta}\langle a_{z\zeta}\rangle_e),\\
\frac{\mathrm{d}L}{\mathrm{d}\tau} &= \varepsilon\big\{(1-\alpha)\Phi_0(D_0^{\xi}\langle a_{z\xi}\rangle_e + D_0^{\zeta}\langle a_{z\zeta}\rangle_e) -\\
&\quad -\alpha\cos\rho\Phi_1\big[D_1^{\xi}(\langle a_{z\xi}^2\rangle_e - \langle a_{z\eta}^2\rangle_e) + D_1^{\zeta}(\langle a_{z\zeta}^2\rangle_e - \langle a_{z\eta}^2\rangle_e)\big]\big\}. \qquad (6)
\end{aligned}
$$

For the secular components in (6) we use a notation that coincides with the corresponding variables; $\langle a\rangle_e$ is the average of $a(\varphi(\tau), \vartheta(\tau), \psi(\tau))$ in the Euler-Poinsot motion,

$$
\begin{aligned}
D_0^{\xi} &= \sum_{j=1}^{N} s_j d_{j\xi}, \quad D_1^{\xi} = \sum_{j=1}^{N} s_j d_{j\xi} n_{j\xi}, \quad D_2^{\xi} = \sum_{j=1}^{N} s_j (d_{j\zeta} n_{j\eta} - d_{j\eta} n_{j\zeta}),\\
D_0^{\zeta} &= \sum_{j=1}^{N} s_j d_{j\zeta}, \quad D_1^{\zeta} = \sum_{j=1}^{N} s_j d_{j\zeta} n_{j\zeta}, \quad D_2^{\zeta} = \sum_{j=1}^{N} s_j (d_{j\eta} n_{j\xi} - d_{j\xi} n_{j\eta}),\\
\Phi_0 &= \frac{(1-e^2)^{3/2}}{\pi}\int_0^{\pi} \frac{g(r(\nu))\mathrm{d}\nu}{(1+e\cos\nu)^2},\\
\Phi_1 &= \frac{(1-e^2)^{3/2}}{\pi}\int_0^{\pi} \frac{\cos\nu\, g(r(\nu))\mathrm{d}\nu}{(1+e\cos\nu)^2}.
\end{aligned}
$$

In the last two formulae we integrate over the true anomaly ν.

If $1/\theta_A \leqslant w < 1$ (SAM motion), then

$$
\begin{aligned}
\langle a_{z\xi}\rangle_e &= \pm\sqrt{\frac{\theta_A(1-\theta_C w)}{\theta_A-\theta_C}}\frac{\pi}{2K(k)}, \qquad \langle a_{z\zeta}\rangle_e = 0,\\
\langle a_{z\xi}^2\rangle_e &= \frac{\theta_A(1-\theta_C w)}{\theta_A-\theta_C}\frac{E(k)}{K(k)}, \qquad \langle a_{z\eta}^2\rangle_e = \frac{1-\theta_C w}{1-\theta_C}\left(1-\frac{E(k)}{K(k)}\right),\\
\langle a_{z\zeta}^2\rangle_e &= \frac{\theta_C(\theta_A w-1)}{\theta_A-\theta_C}\left[1-\frac{1}{k^2}\left(1-\frac{E(k)}{K(k)}\right)\right],
\end{aligned}
$$

where $K(k)$ and $E(k)$ are complete elliptic integrals of the first and second kind with modulus

$$
k = \sqrt{\frac{(1-\theta_C)(1-\theta_A w)}{(1-\theta_A)(1-\theta_C w)}}.
$$

The value $\langle a_{z\xi}\rangle_e$ is positive for SAM_+ motions and negative for SAM_- motions.

If $1 < w \leqslant 1/\theta_C$ (LAM motion)

$$\langle a_{z\xi}\rangle_e = 0, \qquad \langle a_{z\zeta}\rangle_e = \pm\sqrt{\frac{\theta_C(\theta_A w - 1)}{\theta_A - \theta_C}}\frac{\pi}{2K(k)},$$

$$\langle a^2_{z\xi}\rangle_e = \frac{\theta_A(1-\theta_C w)}{\theta_A - \theta_C}\left[1 - \frac{1}{k^2}\left(1 - \frac{E(k)}{K(k)}\right)\right],$$

$$\langle a^2_{z\eta}\rangle_e = \frac{1-\theta_A w}{1-\theta_A}\left(1 - \frac{E(k)}{K(k)}\right), \qquad \langle a^2_{z\zeta}\rangle_e = \frac{\theta_C(\theta_A w - 1)}{\theta_A - \theta_C}\frac{E(k)}{K(k)},$$

$$k = \sqrt{\frac{(1-\theta_A)(1-\theta_C w)}{(1-\theta_C)(1-\theta_A w)}}.$$

The sign of $\langle a_{z\zeta}\rangle_e$ depends on whether the motion belongs to LAM_+ or LAM_-.

The evolutionary equations for SAM and LAM have the same structure. To demonstrate this, one can rewrite Equations (6) in the following concise form:

$$\frac{\mathrm{d}\mathbf{u}}{\mathrm{d}\tau} = \begin{cases} \varepsilon\mathcal{F}_{\pm}(\theta_A, \theta_C, D^{\xi}_{0,1,2}, D^{\zeta}_{1,2}, \mathbf{u}), & \text{motion} \in \mathrm{SAM}_{\pm}\left(\frac{1}{\theta_A} \leqslant w < 1\right); \\ \varepsilon\mathcal{F}_{\pm}(\theta_C, \theta_A, D^{\zeta}_{0,1,2}, D^{\xi}_{1,2}, \mathbf{u}), & \text{motion} \in \mathrm{LAM}_{\pm}\left(1 < w \leqslant \frac{1}{\theta_C}\right). \end{cases}$$

Here $\mathbf{u} = (w, \rho, \sigma, L)^T$, $\mathcal{F}_{\pm}$ is a certain vector-function depending on $\mathbf{u}$, the nucleus' inertia ellipsoid, and sublimation parameters.

Like the initial system (5), system (6) is reversible: if

$$(w(\tau), \rho(\tau), \sigma(\tau), L(\tau))^T$$

is a solution, then

$$(w(-\tau), \pi - \rho(-\tau), \pi + \sigma(-\tau), L(-\tau))^T$$

is also a solution of (6).

3.4. PARAMETERS DEFINING THE BEHAVIOR OF SOLUTIONS OF THE EVOLUTIONARY EQUATIONS

The parameters $D^{\xi,\zeta}_0$, $D^{\xi,\zeta}_1$, $D^{\xi,\zeta}_2$ in (6) are integral characteristics of the comet matter sublimation. If the nucleus is ellipsoidal and physical properties of its surface do not vary too strongly (the distributed mass ejection model), the values of these parameters satisfy

$$|D^{\xi,\zeta}_0| \sim |D^{\xi,\zeta}_2| \ll |D^{\xi,\zeta}_1|.$$

If mass ejection is localized over a small region of the surface,

$$|D^{\xi}_0| \geqslant |D^{\xi}_1|, \quad |D^{\zeta}_0| \geqslant |D^{\zeta}_1|.$$

TABLE II
Values of Φ_0, Φ_1 for some comets

Comet	e	q	Φ_0	Φ_1
2P/Encke	0.846	0.341	0.336	0.097
46P/Wirtanen	0.652	1.063	0.068	0.039
9P/Tempel 1	0.519	1.500	0.040	0.027
19P/Borrelly	0.624	1.358	0.037	0.025
1P/Halley	0.967	0.587	0.0084	0.0040
109P/Swift-Tuttle	0.9635	0.958	0.0026	0.0016

Note: The comets orbital parameters are according to Marsden and Williams (1996).

Parameters Φ_0 and Φ_1 are functions of the perihelion distance q and the eccentricity e. In Table II, values of Φ_0 and Φ_1 are presented for the comets listed in Table I. At large eccentricities ($e \approx 1$) one can use the approximate formulae

$$\Phi_0 \approx (1-e^2)^{3/2}\Psi_0(q), \quad \Phi_1 \approx (1-e^2)^{3/2}\Psi_1(q),$$

where

$$\Psi_0(q) = \frac{1}{\pi}\int_0^\pi g\left(\frac{2q}{1+\cos\nu}\right)\frac{d\nu}{(1+\cos\nu)^2},$$
$$\Psi_1(q) = \frac{1}{\pi}\int_0^\pi g\left(\frac{2q}{1+\cos\nu}\right)\frac{\cos\nu\, d\nu}{(1+\cos\nu)^2}.$$

Values of functions $\Psi_0(q)$, $\Psi_1(q)$ for several values of q are given in Table III. A more detailed analysis of the properties of these functions can be found in Neishtadt et al. (2002).

3.5. PROBABILISTIC INTERPRETATION OF CHANGES IN NUCLEUS ROTATION MODE

When $\varepsilon \neq 0$, changes in the mode of rotation can occur in the motions described by (5). At $w \approx 1$ one of the following transitions can take place, depending on initial conditions:

$$\mathrm{SAM}_\pm \to \mathrm{SAM}_\mp, \quad \mathrm{LAM}_\pm \to \mathrm{LAM}_\mp,$$
$$\mathrm{SAM} \to \mathrm{LAM}, \quad \mathrm{LAM} \to \mathrm{SAM}.$$

A change in the mode of rotation implies that the phase trajectory of (5) crosses the separatrix which separates the different modes at $\varepsilon = 0$. In some cases even a small variation in initial conditions can affect the new mode's type (Figure 4). Following Neishtadt (1991), one can define the probabilities of various modes after

TABLE III
Values of Ψ_0, Ψ_1 for some q

q	Ψ_0	Ψ_1	Ψ_0/Ψ_1
0.5	0.6975	0.3164	2.2047
0.6	0.4465	0.2221	2.0101
0.7	0.3028	0.1632	1.8558
0.8	0.2140	0.1236	1.7305
0.9	0.1556	0.0956	1.6269
1.0	0.1155	0.0750	1.5402
1.1	0.0870	0.0593	1.4670
1.2	0.0661	0.0471	1.4048
1.3	0.0505	0.0373	1.3516
1.4	0.0385	0.0295	1.3061
1.5	0.0293	0.0231	1.2672
1.6	0.0222	0.0180	1.2337
1.7	0.0166	0.0137	1.2051
1.8	0.0122	0.0103	1.1806
1.9	0.0089	0.0076	1.1597
2.0	0.0063	0.0055	1.1419

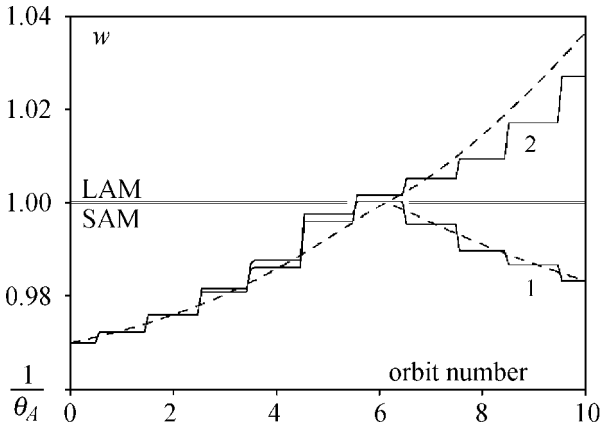

Figure 4. An example of change of mode at a separatrix crossing: $SAM_+ \to SAM_-$ (curve 1) and $SAM_+ \to LAM_+$ (curve 2). The initial conditions in the motions 1 and 2 differ only in the value of φ: $\varphi(0) = 120.0°$ in the motion 1 and $\varphi(0) = 0.0°$ in the motion 2. Values of the other parameters at $\tau = 0$ coincide in both the cases: $L(0) = 1.000$, $\rho(0) = 45.0°$, $\sigma(0) = \psi(0) = 90.0°$. Values of A, B, C, ε are equal to those given in Sections 2 and 3 for comet Halley. Orbital parameters are also the same as for comet Halley. Intensity distribution and position of active areas on the nucleus' surface correspond to the first Halley-like model nucleus discussed in Section 5.

separatrix crossing, but, unfortunately, methods for calculating these probabilities in multi-frequency systems have not been developed (in Neishtadt (1991) only single-frequency systems were considered).

The evolutionary equations (6) in the limit $w \to 1$ can be used to describe the behavior of phase trajectories before and after a change in mode, but they cannot be used to study phenomena that occur during the separatrix crossing.

3.6. CONDITIONS FOR THE AVERAGING APPROXIMATION

Application of the averaging approximation rests on the assumption that the variations in the rotational parameters over one orbit around the Sun are small enough. Numerical integration of Equations (5) affirms this assumption for typical values of parameters of the comet nucleus and the orbit elements, given in Tables I and II. More on that subject can be found in Neishtadt et al. (2002).

The averaging approximation also assumes that capture into resonance does not take place. Rigorous results on the application of the averaging method in multi-frequency systems, presented in Arnold (1978) and Arnold et al. (1988), imply that Equations (6) generally describe the evolution of nucleus rotation for the majority of initial conditions. The set of initial conditions where this is not true (whose measure tends to 0 as $\varepsilon \to 0$) consists mainly of those corresponding to solutions captured into a resonance. In this case a commensurability between frequencies of the perturbed Euler-Poinsot motion is preserved for a long time. To study solutions of (5) when a commensurability exists one can use the approach described in Arnold et al. (1988). Taking into account the above mentioned 'non-generality' of resonant motions, we do not consider them in the present paper.

3.7. EVOLUTIONARY EQUATIONS FOR NUCLEI WITH NEARLY AXISYMMETRIC INERTIA ELLIPSOIDS

In Neishtadt et al. (2002), the rotational evolution of a comet nucleus was studied under the assumption that its inertia ellipsoid was axially symmetric. In this subsection we show that the equations derived by Neishtadt et al. (2002) can be obtained as a limiting case of our current equations.

Here we only consider the case of a prolate nuclei:

$$\theta_A - 1 \ll 1 - \theta_C. \tag{7}$$

Use the parameter $\bar{\varepsilon} = \theta_A - 1$ to describe the proximity of the inertia ellipsoid to an axially symmetric one. If $w \in (1, 1/\theta_C)$, $w - 1 > c_0^{-1}$ (where c_0 is a positive constant that can be chosen arbitrarily large), then at sufficiently small values of $\bar{\varepsilon}$ the nutation angle oscillates with a small amplitude and the period T_ϑ around its

mean value $\bar{\vartheta}$:

$$\vartheta = \bar{\vartheta} + O(\bar{\varepsilon}),\ \bar{\vartheta} = \begin{cases} \arccos \dfrac{\theta_A(w-1)}{1-\theta_C} + O(\bar{\varepsilon}) & \text{for LAM}_+; \\ \pi - \arccos \dfrac{\theta_A(w-1)}{1-\theta_C} + O(\bar{\varepsilon}) & \text{for LAM}_-. \end{cases} \tag{8}$$

The condition $w - 1 > c_0^{-1}$ ensures that the polhode is far from the separatrices bounding the $\text{SAM}_\pm$ regions.

The angle $\bar{\vartheta}$ can be used instead of w as a parameter in the LAM family. Changing variables $w \to \bar{\vartheta}$, we rewrite (6) as follows:

$$\begin{aligned} \frac{\mathrm{d}\bar{\vartheta}}{\mathrm{d}\tau} &= \frac{\varepsilon}{2L}\left[3\alpha\Phi_1 D_1^\zeta \cos\rho \cos\bar{\vartheta} - 2(1-\alpha)\Phi_0 D_0^\zeta\right]\sin\bar{\vartheta} + O(\varepsilon\bar{\varepsilon}), \\ \frac{\mathrm{d}\rho}{\mathrm{d}\tau} &= -\frac{\varepsilon\alpha \sin\rho}{4L} D_1^\zeta \Phi_1 (2 - 3\sin^2\bar{\vartheta}) + O(\varepsilon\bar{\varepsilon}), \\ \frac{\mathrm{d}\sigma}{\mathrm{d}\tau} &= \frac{\varepsilon\alpha}{2L} D_2^\zeta \Phi_1 \cos\bar{\vartheta} + O(\varepsilon\bar{\varepsilon}), \\ \frac{\mathrm{d}L}{\mathrm{d}\tau} &= -\frac{\varepsilon}{2}\left[\alpha\Phi_1 D_1 (2 - 3\sin^2\bar{\vartheta})\cos\rho - 2(1-\alpha)\Phi_0 D_0 \cos\bar{\vartheta}\right] + O(\varepsilon\bar{\varepsilon}). \end{aligned} \tag{9}$$

Equations (9) at $\bar{\varepsilon} = 0$ coincide with the evolutionary equations in Neishtadt et al. (2002). This implies that the conclusions about secular effects in nucleus motion made in Neishtadt et al. (2002) are also valid in the case when the inertia ellipsoid is slightly different from an axially symmetric one ($\bar{\varepsilon} \ll 1$).

Equations describing the evolution of the SAM state cannot be simplified like this for $\bar{\varepsilon} \ll 1$. Even in the absence of perturbations ($\varepsilon = 0$), motions with $\vartheta \approx 90^\circ$ are essentially different at $\bar{\varepsilon} = 0$ and $\bar{\varepsilon} \neq 0$.

4. Quasi-stationary Motions

An important property of (6) is the independence of its right-hand side from the variable σ. This is due to symmetry of the moments applied to the nucleus before and after passage through the perihelion. Moreover, taking the independent variable as

$$\tau_* = \Phi_1 \int_0^\tau \frac{\mathrm{d}\tau'}{L},$$

one obtains in (6) a closed subsystem for w and ρ:

$$\begin{aligned} \frac{\mathrm{d}w}{\mathrm{d}\tau_*} \;=\; & 2\varepsilon\left\{(1-\alpha)\Phi_0\left[D_0^\xi\langle a_{z\xi}\rangle_e\left(\frac{1}{\theta_A} - w\right) + D_0^\zeta\langle a_{z\zeta}\rangle_e\left(\frac{1}{\theta_C} - w\right)\right] - \right. \\ & -\alpha\cos\rho\,\Phi_1\left[D_1^\xi\left(\left(\frac{1}{\theta_A} - w\right)\langle a_{z\xi}^2\rangle_e - (1-w)\langle a_{z\eta}^2\rangle_e\right) + \right. \\ & \left.\left. + D_1^\zeta\left(\left(\frac{1}{\theta_C} - w\right)\langle a_{z\zeta}^2\rangle_e - (1-w)\langle a_{z\eta}^2\rangle_e\right)\right]\right\}, \end{aligned}$$

$$\frac{\mathrm{d}\rho}{\mathrm{d}\tau_*} = -\frac{\varepsilon\alpha\,\sin\rho\,\Phi_1}{2}\left[D_1^{\xi}\left(\langle a_{z\xi}^2\rangle_e - \langle a_{z\eta}^2\rangle_e\right) + D_1^{\zeta}\left(\langle a_{z\zeta}^2\rangle_e - \langle a_{z\eta}^2\rangle_e\right)\right]. \tag{10}$$

If (w^*, ρ^*) is a stationary solution of (10), one can substitute (w^*, ρ^*) into the last two equations of (6) to construct a quasi-stationary solution of the evolutionary equations:

$$\mathbf{u}^* = (w^*, \rho^*, \sigma^*(\tau), L^*(\tau))^{\mathrm{T}}. \tag{11}$$

In quasi-stationary motions (11) the nucleus angular momentum increases or decreases linearly:

$$L^*(\tau) = \varepsilon c_L \tau + L_0^*,$$

where L_0^* is its initial value,

$$c_L = (1-\alpha)\Phi_0(D_0^{\xi}\langle a_{z\xi}\rangle_e + D_0^{\zeta}\langle a_{z\zeta}\rangle_e) - \\ -\alpha\,\cos\,\rho\Phi_1\left[D_1^{\xi}\left(\langle a_{z\xi}^2\rangle - \langle a_{z\eta}^2\rangle\right) + D_1^{\zeta}\left(\langle a_{z\zeta}^2\rangle - \langle a_{z\zeta}^2\rangle\right)\right]\Big|_{w=w^*,\rho=\rho^*}.$$

For a more detailed description of other properties of quasi-stationary motions we divide them into three classes.

Class A: trivial quasi-stationary motions. For all values of the parameters $D_0^{\xi,\zeta}$, $D_1^{\xi,\zeta}$, $\Phi_{0,1}$ there exist degenerate quasi-stationary motions with the angular momentum vector directed along the OZ axis ($\sin\rho^* = 0$) and a simple SAM ($w^* = 1/\theta_A$) or simple LAM ($w^* = 1/\theta_C$) rotation mode. If

$$|\kappa_\xi| > \kappa_0, \quad \kappa_\xi = \frac{\Phi_0 D_0^{\xi}}{\Phi_1 D_1^{\xi}}, \quad \kappa_0 = \frac{3\alpha}{2(1-\alpha)},$$

there are simple SAM motions of Class A that are stable with respect to variables w^*, ρ^*. If

$$|\kappa_\zeta| > \kappa_0,\ \kappa_\zeta = \frac{\Phi_0 D_0^{\zeta}}{\Phi_1 D_1^{\zeta}}$$

there are simple LAM motions that are stable in the same sense. More detailed information on the stable motions of Class A are given in Table IV.

Class B. The angular momentum vector is parallel to the radius vector of the comet at the perihelion ($\mathbf{L} \uparrow\uparrow \mathbf{r}_\pi$ or $\mathbf{L} \uparrow\downarrow \mathbf{r}_\pi$). The point where the straight line containing the nucleus' angular velocity vector crosses its inertia ellipsoid moves faster and faster ($c_L > 0$) or slower and slower ($c_L < 0$) along the polhode

TABLE IV
Stability conditions for motions of the Class A

Motion	Stability conditions
$\rho^* = 0(\mathbf{L} \uparrow\uparrow \mathbf{r}_\pi)$	
$w_* = \frac{1}{\theta_A}$	
Simple SAM$_+$	$D_1^\xi > 0,\ \kappa_\xi > \kappa_0$
Simple SAM$_-$	$D_1^\xi > 0,\ \kappa_\xi < -\kappa_0$
$w_* = \frac{1}{\theta_C}$	
Simple LAM$_+$	$D_1^\zeta > 0,\ \kappa_\zeta > \kappa_0$
Simple LAM$_-$	$D_1^\zeta > 0,\ \kappa_\zeta < -\kappa_0$
$\rho^* = \pi(\mathbf{L} \uparrow\downarrow \mathbf{r}_\pi)$	
$w_* = \frac{1}{\theta_A}$	
Simple SAM$_+$	$D_1^\xi < 0,\ \kappa_\xi < -\kappa_0$
Simple SAM$_-$	$D_1^\xi < 0,\ \kappa_\xi > \kappa_0$
$w_* = \frac{1}{\theta_C}$	
Simple LAM$_+$	$D_1^\zeta < 0,\ \kappa_\zeta < -\kappa_0$
Simple LAM$_-$	$D_1^\zeta < 0,\ \kappa_\zeta > \kappa_0$

corresponding to the unperturbed motion at $w = w^*$ (SAM at $w^* < 1$ and LAM at $w^* > 1$).

Quasi-stationary complex SAMs of Class B exist if

$$\kappa_\xi^* < |\kappa_\xi| < \kappa_\xi^{**}, \tag{12}$$

where

$$\kappa_\xi^* = \inf_{w\in(\frac{1}{\theta_A},1)} \frac{\alpha|G_\xi(w) + \chi G_\zeta(w)|}{(1-\alpha)F_\xi(w)},$$

$$\kappa_\xi^{**} = \sup_{w\in(\frac{1}{\theta_A},1)} \frac{\alpha|G_\xi(w) + \chi G_\zeta(w)|}{(1-\alpha)F_\xi(w)},$$

$$G_\xi(w) = \left(\frac{1}{\theta_A} - w\right)\langle a_{z\xi}^2\rangle_e - (1-w)\langle a_{z\eta}^2\rangle_e,$$

$$G_\zeta(w) = \left(\frac{1}{\theta_C} - w\right)\langle a_{z\zeta}^2\rangle_e - (1-w)\langle a_{z\eta}^2\rangle_e,$$

$$F_\xi(w) = |\langle a_{z\xi}\rangle_e|\left(w - \frac{1}{\theta_A}\right),\ \chi = \frac{D_1^\zeta}{D_1^\xi}.$$

Condition (12) ensures that at sin $\rho^* = 0$ and $w = w^* \in (1/\theta_A, 1)$ the right-hand side of the first equation in (10) is zero.

One can similarly write the condition for existence of complex LAMs of Class B:

$$\kappa_\zeta^* < |\kappa_\zeta| < \kappa_\zeta^{**}, \tag{13}$$

where

$$\kappa_\zeta^* = \inf_{w\in(1,\frac{1}{\theta_C})} \frac{\alpha|(G_\xi(w)/\chi) + G_\zeta(w)|}{(1-\alpha)F_\zeta(w)},$$

$$\kappa_\zeta^{**} = \sup_{w\in(1,\frac{1}{\theta_C})} \frac{\alpha|(G_\xi(w)/\chi) + G_\zeta(w)|}{(1-\alpha)F_\zeta(w)},$$

$$F_\zeta(w) = |\langle a_{z\zeta}\rangle_e|\left(\frac{1}{\theta_C} - w\right).$$

Class C. The nucleus' angular momentum vector $\mathbf{L}$ precesses at a constant angle ρ^* around the OZ axis, which is parallel to the comet's radius vector at the perihelion. The rate of the precession can be obtained from the third equation in (6)

$$\frac{\mathrm{d}\sigma^*}{\mathrm{d}\tau} = \frac{\varepsilon c_\sigma}{L^*(\tau)}, \tag{14}$$

where

$$c_\sigma = \frac{\alpha\Phi_1}{2}(D_2^\xi\langle a_{z\xi}\rangle_e + D_2^\zeta\langle a_{z\zeta}\rangle_e)|_{w=w^*}.$$

It follows from (14) that the precession rate grows as the nucleus rotation slows down ($c_L < 0$) and decreases as the nucleus rotation accelerates ($c_L > 0$).

The nucleus' motion with respect to the angular momentum vector (SAM at $w^* < 1$ and LAM at $w^* > 1$) is exactly the same as in motions of Class B.

The value of w^* in Class C motions should satisfy the condition

$$\frac{H_\xi(w^*)}{H_\zeta(w^*)} = -\chi, \tag{15}$$

where

$$H_\xi(w) = \langle a_{z\xi}^2\rangle_e - \langle a_{z\eta}^2\rangle_e, \quad H_\zeta(w) = \langle a_{z\zeta}^2\rangle_e - \langle a_{z\eta}^2\rangle_e.$$

Assume it is possible to select w^* to satisfy condition (15) at a certain value of χ. If $w^* \in (1/\theta_A, 1)$, then a quasi-stationary motion of Class C exists provided that

$$|\kappa_\xi| < \frac{\alpha|G_\xi(w^*) + \chi G_\zeta(w^*)|}{(1-\alpha)F_\xi(w^*)}.$$

If $w^* \in (1, 1/\theta_C)$, then the condition of existence of Class C motion takes the form:

$$|\kappa_\zeta| < \frac{\alpha|(G_\xi(w^*)/\chi) + G_\zeta(w^*)|}{(1-\alpha)F_\zeta(w^*)}.$$

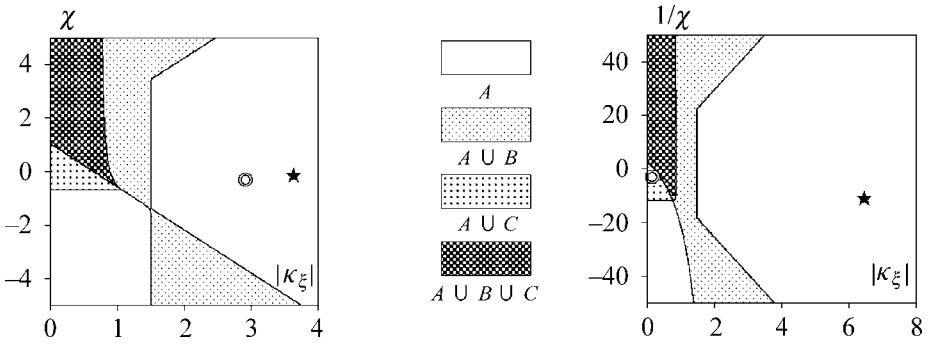

Figure 5. Classification of quasi-stationary SAMs (left) and LAMs (right), existing at corresponding values of parameters $\kappa_\xi, \kappa_\zeta, \chi$. The values of these parameters for the first and second variants of active zones relative intensities for model Halley nucleus (Section 5) are marked with the symbols ⋆ and ○ correspondingly.

It follows that the types of quasi-stationary motions that can exist for a nucleus with a certain given distribution of active zones depend on the values of parameters $\chi, \kappa_\xi, \kappa_\zeta$ (properties of quasi-stationary SAMs depend on χ, κ_ξ; properties of LAMs depend on χ, κ_ζ).

In Figure 5 we present the separation of the set of values of these parameters into areas with different combinations of possible quasi-stationary motions for a nucleus with moment of inertia ratios equal to those for comet Halley (Section 2).

The type of quasi-stationary motions is important for classification. It can be used to distinguish nuclei with different scenarios of rotational evolution. We suppose that a more detailed description of the diversity of such scenarios would be a formal exercise, due to very rough correspondence between the empirical mass ejection model and the real processes. Therefore, we restrict ourselves to consider several examples based on spacecraft observations of the nuclei of comets Halley and Borrelly.

5. Evolutionary Paths for a Halley-like Nucleus

It was shown by Belton et al. (1991) that, based on the images of the comet Halley nucleus transmitted by the 'Vega 1,2' and 'Giotto' spacecraft, one can conclude that there are five active zones. We consider the dynamics of rotation for various intensities of mass ejection at these zones.

Suppose that the centers of the active zones are the points on the nucleus surface presented in Table V. Within the accuracy to which the active zones can be identified, this assumption agrees with the results by Belton et al. (1991). The nucleus of comet Halley is essentially non-convex (Figure 1). However, for this distribution of active zones one can neglect effects due to the shadowing of the zones with other parts of the nucleus. Indeed, based on ideas of Gutierrez et al. (2000), we take the following parameter to describe shadowing of the jth face:

$$\delta_j^* = \min_{\mathbf{e}\in\mathcal{E}_j}[\arccos(\mathbf{n}_j, \mathbf{e})],$$

TABLE V

Position and orientation of the active zones for Halley-like model nucleus

Zone 1	$\mathbf{R}_1$	$R_*(-0.22059, 0.28199, -1.44677)^{\mathrm{T}}_{O\xi\eta\zeta}$
	$\mathbf{n}_1$	$(-0.32714, 0.85784, -0.39936)^{\mathrm{T}}_{O\xi\eta\zeta}$
Zone 2	$\mathbf{R}_2$	$R_*(0.19626, 0.39703, 0.97325)^{\mathrm{T}}_{O\xi\eta\zeta}$
	$\mathbf{n}_2$	$(0.04046, 0.61546, 0.78713)^{\mathrm{T}}_{O\xi\eta\zeta}$
Zone 3	$\mathbf{R}_3$	$R_*(-0.46986, -0.43157, 0.99487)^{\mathrm{T}}_{O\xi\eta\zeta}$
	$\mathbf{n}_3$	$(-0.87622, -0.41999, 0.23632)^{\mathrm{T}}_{O\xi\eta\zeta}$
Zone 4	$\mathbf{R}_4$	$R_*(0.17474, 0.77468, -0.26201)^{\mathrm{T}}_{O\xi\eta\zeta}$
	$\mathbf{n}_4$	$(0.15729, 0.93500, -0.31786)^{\mathrm{T}}_{O\xi\eta\zeta}$
Zone 5	$\mathbf{R}_5$	$R_*(0.31496, -0.61161, -0.72302)^{\mathrm{T}}_{O\xi\eta\zeta}$
	$\mathbf{n}_5$	$(0.24348, -0.96664, -0.07947)^{\mathrm{T}}_{O\xi\eta\zeta}$

where ε_j is a set of unit vectors defining directions from the center of this face to points of the nucleus' surface belonging to the edges of the approximating polyhedron. If the angle δ_j between the outer normal $\mathbf{n}_j$ and the direction to the Sun is smaller than δ_j^*, the center of the face is lighted at any orientation of the nucleus satisfying this condition. In particular, in the case $\delta_j^* = 90^\circ$ the face belongs to the convex part of the nucleus' surface (or, more rigorously, to the convex hull of the approximating polyhedron), and it cannot be shadowed for $\delta_j < 90^\circ$.

According to our calculations, for Halley nucleus model in use and accepted positions of active zones we have

$$\delta_1^* = \delta_2^* = \delta_5^* = 90^\circ, \quad \delta_3^* = 86^\circ, \quad \delta_4^* = 87^\circ.$$

Therefore, only active zones 3 and 4 can be shadowed. However, the range of angles where (4) cannot be applied due to the shadowing effects is quite small (less than 4°). Hence, the difference between the averaged equations obtained with the use of (4) and its hypothetical modification taking shadowing effects into account is insignificant. Moreover, this difference is absolutely unimportant because of very approximate correspondence of the accepted matter sublimation model and the real processes.

We consider two possible cases for the zone activity levels (values of the integral parameters of mass ejection are shown in Table VI). The first case is the most probable for the nucleus of comet Halley and was suggested in Belton et al. (1991):

$$s_1 = s_4 = \frac{1}{3}, \quad s_2 = s_3 = s_5 = \frac{1}{9}.$$

The phase portrait of system (10) showing secular evolution of variables w and ρ as such a distribution of the intensities is shown in Figure 6.

TABLE VI
Dynamic parameters of Halley-like model nucleus

Description	Variant 1	Variant 2
Integral mass ejection parameters		
D_0^{ξ}	−0.30703	−0.21455
D_1^{ξ}	0.17284	0.15312
D_2^{ξ}	−0.09872	−0.12508
D_0^{ζ}	0.04422	−0.00365
D_1^{ζ}	−0.01420	−0.05161
D_2^{ζ}	0.32992	0.27154
Classification parameters		
κ_{ξ}	−3.69341	−2.91326
κ_{ζ}	−6.47612	0.14723
χ	−0.08214	−0.33704

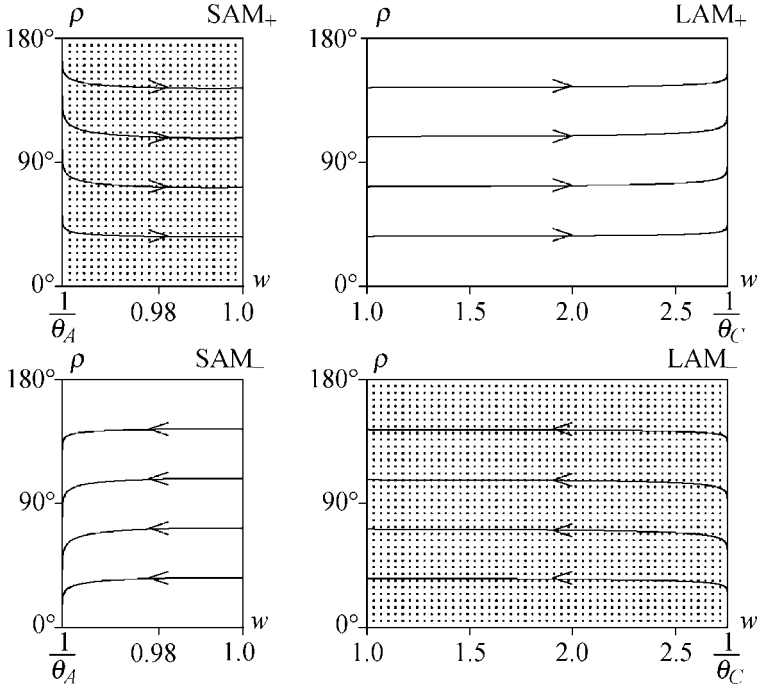

Figure 6. Phase trajectories of (11) at the distribution of intensities of the active zones according to Belton et al. (1991).

The shading denotes a decreasing angular momentum (spin-down). If a phase point $(w(\tau), \rho(\tau))$ is in the non-shaded part of the phase portrait, the nucleus spins up.

Taking into account the behavior of the phase trajectories one can deduce that in the considered case the motions of the class A are stable quasi-stationary modes: simple LAM_+ , $\mathbf{L} \uparrow\downarrow \mathbf{r}_\pi$ and simple SAM_- , $\mathbf{L} \uparrow\uparrow \mathbf{r}_\pi$. Variation of the angular momentum in these motions is described by the formulas

$$\frac{\mathrm{d}L^*}{\mathrm{d}\tau} = \varepsilon \Phi_1 D_1^\zeta \left[(1-\alpha) + \alpha \kappa^\xi\right] \tag{16}$$

and

$$\frac{\mathrm{d}L^*}{\mathrm{d}\tau} = -\varepsilon \Phi_1 D_1^\xi \left[(1-\alpha) + \alpha \kappa^\xi\right] \tag{17}$$

accordingly. Using the parameter values of P/Halley, given in Tables I, II, and VI, one can easily establish that the right-hand sides of Equations (16) and (17) are positive. Therefore, in these quasi-stationary motions the nucleus spins up. Denoting variation of the nucleus angular velocity in the orbital period as $\Delta\boldsymbol{\Omega}$, we find

$$\frac{|\Delta\boldsymbol{\Omega}|}{|\boldsymbol{\Omega}|} \approx \frac{1}{C}\left(\frac{\Omega_*}{\Omega_0}\right)\frac{\mathrm{d}L^*}{\mathrm{d}\tau} \approx 6.1 \cdot 10^{-2} \tag{18}$$

for simple LAM_+ , $\mathbf{L} \uparrow\downarrow \mathbf{r}_\pi$ and

$$\frac{|\Delta\boldsymbol{\Omega}|}{|\boldsymbol{\Omega}|} \approx \frac{1}{A}\left(\frac{\Omega_*}{\Omega_0}\right)\frac{\mathrm{d}L^*}{\mathrm{d}\tau} \approx 0.13 \tag{19}$$

for simple SAM_-, $\mathbf{L} \uparrow\uparrow \mathbf{r}_\pi$. Symbol Ω_0 in (18) and (19) denotes the comet mean motion.

Now let us consider the case of the mass ejection primarily from active zones 1 and 2:

$$s_1 = \frac{1}{3}, \quad s_2 = \frac{1}{2}, \quad s_3 = s_4 = s_5 = \frac{1}{18}.$$

The phase portrait of system (10) for such a nucleus is shown in Figure 7. Together with a stable quasi-stationary motion of Class A (simple SAM_-, $\mathbf{L} \uparrow\uparrow \mathbf{r}_\pi$) there also exists a stable quasi-stationary motion of Class C, that is complex LAM_- ($w^* \approx 1.532$). In this latter motion, the angle between angular momentum vector $\mathbf{L}$ and vector $\mathbf{r}_\pi$ is $\approx 99.8^\circ$. The rate of precession of the angular momentum vector around OZ-axis can be estimated as follows:

$$\frac{\mathrm{d}\sigma^*}{\mathrm{d}t} \sim \varepsilon \Phi_1 D_2^\zeta \Omega_* \sim 10^\circ \text{ per orbital period}$$

Note that at $w^* \approx 1.532$ the angle ϑ between $\mathbf{L}$ and the axis $O\zeta$ of the body-fixed coordinate system varies from $\approx 55.5^\circ$ to $\approx 56.5^\circ$.

These examples demonstrate that evolution depends not only on the location of active zones, but on their respective intensities as well.

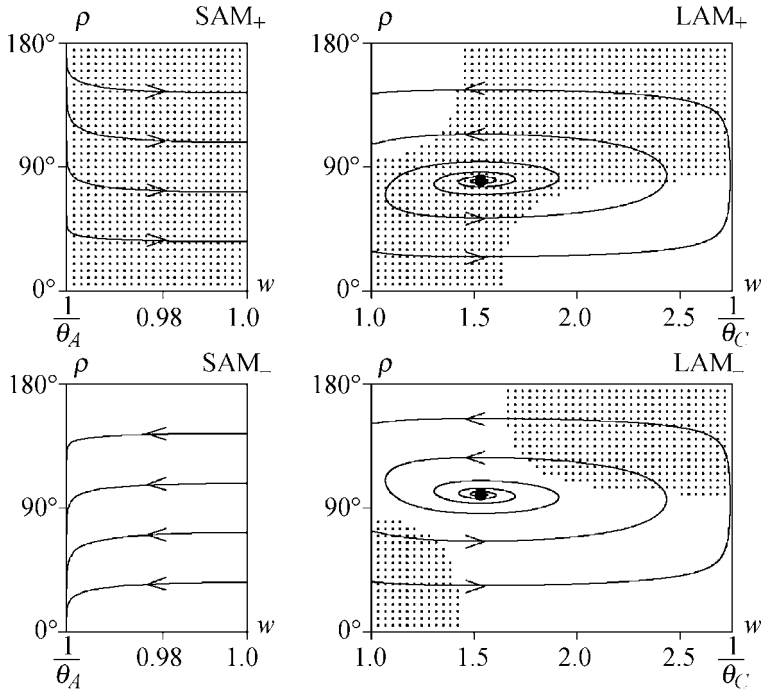

Figure 7. Phase trajectories of (11) for Halley-like nucleus with principal mass ejection in the active zones 1 and 2.

6. Dynamic Properties of a Borrelly-like Nucleus

Detailed images of the nucleus of comet 19P/Borrelly were obtained by the 'Deep Space-1' mission (Kerr, 2001). Approximate reconstruction of the nucleus' shape based on these images and observations by Hubble Space Telescope (Lamy et al., 1998) is shown in Figure 8. The nucleus can be approximated as a combination of two ellipsoids with major semi-axes 1.6, 1.8, 3.0 km and 0.96, 1.08, 1.8 km accordingly. The distance between the centers of these ellipsoids is 3.7 km. Assuming that the nucleus is homogeneous, one obtains:

$$\theta_A = 1.03038, \quad \theta_C = 0.25886.$$

The images indicate the existence of three active zones in the middle region of the nucleus. Assume for definiteness that in the body-fixed reference frame $O\xi\eta\zeta$ the centers of these active zones are defined by radius-vectors $\mathbf{R}_1, \mathbf{R}_2, \mathbf{R}_3$ presented in Table VII. The parameters of mass ejection calculated for the case of equal intensities of the zones have the following values:

$$D_0^\xi = 0.00211, \quad D_1^\xi = 0.00202, \quad D_2^\xi = 0.01394,$$

$$D_0^\zeta = -0.00218, \quad D_1^\zeta = -0.00043, \quad D_2^\zeta = -0.04985.$$

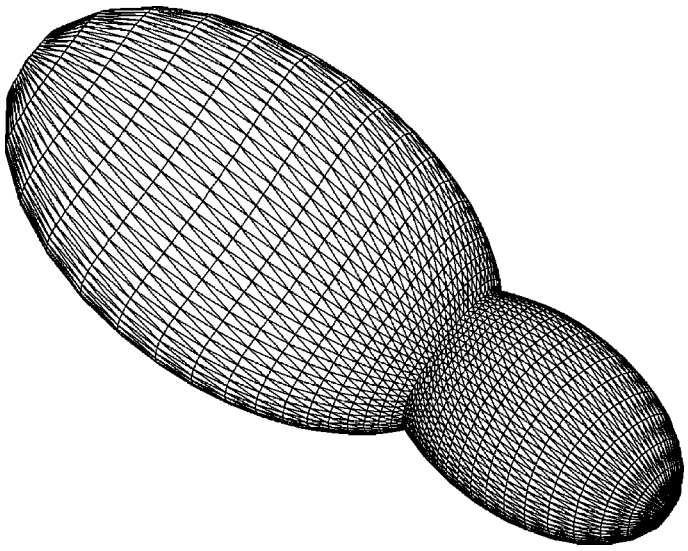

Figure 8. P/Borrelly nucleus: rough reconstruction based on Deep Space-1 images.

TABLE VII

Position and orientation of the active zones for Borrelly-like model nucleus

Zone 1	$\mathbf{R}_1$	$R_*(-0.36292, 0.10853, -0.40400)^{\mathrm{T}}_{O\xi\eta\zeta}$
	$\mathbf{n}_1$	$(0.95555, 0.23511, 0.17789)^{\mathrm{T}}_{O\xi\eta\zeta}$
Zone 2	$\mathbf{R}_2$	$R_*(0.35606, 0.01017, -0.31896)^{\mathrm{T}}_{O\xi\eta\zeta}$
	$\mathbf{n}_2$	$(0.96787, 0.03299, 0.24927)^{\mathrm{T}}_{o\xi\eta\zeta}$
Zone 3	$\mathbf{R}_3$	$R_*(0.36711, -0.08721, -0.40252)^{\mathrm{T}}_{O\xi\eta\zeta}$
	$\mathbf{n}_3$	$(0.96978, -0.16768, 0.17722)^{\mathrm{T}}_{O\xi\eta\zeta}$

The main qualitative properties of secular evolution for the nucleus rotation are determined by parameters $\kappa_\xi, \kappa_\zeta, \chi$. In the case considered

$$\kappa_\xi = 1.55418, \quad \kappa_\zeta = 7.59512, \quad \chi = -0.21128.$$

With the use of expressions obtained in Section 4, one can find that this nucleus can perform a stable, quasi-stationary motion of Class A, that is simple SAM with the angular momentum vector directed along the line of apsides. Such a mode of rotation is supposed to be the most probable one for the real P/Borrelly nucleus.

7. Conclusions

Using the averaging method, we obtained evolutionary equations that describe the secular effect of outgassing on the rotation of comet nuclei. We defined parameters that determine the qualitative properties of comet nucleus rotational evolution. Classification of possible quasi-stationary modes of motion was also given.

Acknowledgements

This work was supported by the NASA JURRISS program under Grant NAG5-8715. AIN, AAV, and VVS acknowledge support from Russian Foundation for Basic Researches via Grants 00-15-96146, 00-01-00538 and 00-00-00174 respectively. Also they acknowledge support from INTAS via Grant 00-221. AIN acknowledges support from the INTEGRATION program via Grant B0053. DJS acknowledges support from the PG&G program via Grant NAG5-9017.

Appendix. List of symbols

A_*, B_*, C_* and A, B, C	moments of inertia about axes $O\xi$, $O\eta$, $O\zeta$ respectively and their dimensionless values
$a_{x\xi}, \ldots, a_{z\zeta}$	elements of the transfer matrix between coordinate systems $Oxyz$ and $O\xi\eta\zeta$
$D_0^{\xi,\zeta}$, $D_1^{\xi,\zeta}$, $D_2^{\xi,\zeta}$	integral characteristics of the matter sublimation
$d_{j\xi}, d_{j\eta}, d_{j\zeta}$	geometric characteristics used to compute torques due to sublimation from the jth face
$\mathbf{e}_S$	unit vector pointing to the Sun
$f(\delta_j)$	function describing the dependence of the mass ejection from jth face on local illumination conditions
$g(r)$	function describing the dependence of the mass ejection rate on the heliocentric distance
I_*	$m_* R_*^2$
$\mathbf{L}$	angular momentum vector of the nucleus
$\mathbf{M}^r$	reactive torque due to the ice sublimation from the nucleus surface
M_x^r, M_y^r, M_z^r and M_ξ^r, M_η^r, M_ζ^r	projections of the dimensionless reactive torque onto the corresponding axes of the coordinate systems $Oxyz$ and $O\xi\eta\zeta$
m_*	nucleus mass
$m_{Xx}, \ldots, m_{Zz}$	elements of the transfer matrix between coordinate systems $OXYZ$ and $Oxyz$
$\mathbf{n}_j$	outer normal to the jth face

Q_*	mass ejection rate from a certain hypothetical surface at a heliocentric distance 1 AU
Q_j	mass ejection rate on the jth face
R_*	typical linear dimension of the nucleus
$\mathbf{R}_j$	radius vector of the jth face with respect to the center of mass of the nucleus
r	nucleus heliocentric distance
s_j	relative intensity of the jth face
T	kinetic energy of the rotational motion
$\mathbf{v}_j$	effective velocity of the matter ejection from jth face
w	variable describing the nucleus motion with respect to the angular momentum vector
$w^*, \rho^*, \sigma^*(\tau), L^*(\tau)$	quasi-stationary solution of the evolutionary equations
α	not substantial coefficient in the expression for function $f(\delta)(\approx 1/2)$
δ_j	angle between the outer normal to the jth face and vector $\mathbf{e}_S$
ε	small parameter characterizing the nucleus motion excitation due to the reactive torque
θ_A and θ_C	normalized moments of inertia ($= A/B$ and $= C/B$)
$\kappa_\xi, \kappa_\zeta, \chi$	parameters defining the properties of quasi-stationary motions
ρ, σ	angles used to define the orientation of the nucleus angular momentum $\mathbf{L}$
τ	dimensionless independent variable ($= \Omega_* t$)
$\mathbf{\Phi}_0, \mathbf{\Phi}_1$	integral characteristics of the nucleus heating along the orbit
ϕ, ϑ, ψ	Euler angles used to define the orientation of the system $O\xi\eta\zeta$ with respect to the system $Oxyz$
$\mathbf{\Omega}$	nucleus angular velocity
Ω_*	initial value of $\mathbf{\Omega}$
Ω_0	comet mean motion

References

Arnold, V. I.: 1978, *Mathematical Methods of Classical Mechanics*, Springer, New York.

Arnold, V. I., Kozlov, V. V. and Neishtadt, A. I.: 1998, *Mathematical Aspects of Classical and Celestial Mechanics (Encyclopaedia of Mathematical Science, 3)*, Springer, Berlin.

Beletskii, V. I.: 1966, *Motion of an Artificial Satellite about Its Center of Mass*, Israel Program for Scientific Translations, Jerusalem.

Belton, M. J. S., Julian, W. H., Anderson, A. J. and Mueller, B. E. A.: 1991, 'The spin state and homogeneity of comet Halley's nucleus', *Icarus* **93**, 183–193.

Bogolyubov, N. N. and Mitropolsky, Yu. A.: 1961, *Asymptotic Methods in the Theory of Nonlinear Oscillations*, Gordon and Breach Science Publishers, New York.

Crifo, J. F. and Rodionov, A. V.: 1999, 'Modelling the circumnuclear coma of comets: objectives, methods and recent results', *Planet. Space Sci.* **47**, 797–826.

Dobrovolskis, A. R.: 1996, 'Inertia of any polyhedron', *Icarus* **124**, 698–704.

Gutierrez, P. G., Ortiz, J. L., Rodrigo, R. and López-Moreno, J. J.: 2000, 'A study of water production and temperatures of rotating irregularly shaped cometary nuclei', *Astron. Astrophys.* **355**, 809–817.

Jorda, L. and Licandro, J.: (*in Press*), 'Modeling the rotation of comets', *Proc. IAU Colloquim* 168, Nanjing, China. *Publ. Astron. Soc. Pac*.

Julian, W. H.: 1990, 'The comet Halley nucleus: random jets', *Icarus* **88**, 355–371.

Kamél, L.: 1991, 'The evolution of P/Encke's light curve: no secular fading, a vanishing perihelion asymmetry', *Icarus* **93**, 226–245.

Kerr, R. A.: 2001, 'Close look at the heart of Borrelly', *Science* **294**, 27–28.

Kinoshita, H.: 1992, 'Analytical expansions of torque-free motions for short and long axis modes', *Celest. Mech. & Dyn. Astr.* **53**, 365–375.

Lamy, P. L., Toth, I. and Weaver, H. A.: 1998, 'Hubble Space Telescope observations of the nucleus and inner coma of comet 19P/1904 Y2 (Borrelly)', *Astron. Astrophys*. **337**, 945–954.

Landau, L. D. and Lifshitz, E. M.: 1976, *Mechanics*, Pergamon Press, Oxford.

Marsden, B. G. and Williams, G. V.: 1996, *Catalogue of Cometary Orbits*, Smithsonian Astrophys. Obs., Cambridge.

Marsden, B. G., Sekanina, Z. and Yeomans, D. K.: 1973, 'Comets and nongravitational forces. V', *Astron. J.* **78**, 211–225.

Neishtadt, A. I.: 1991, 'Probability phenomena due to separatrix crossing', *Chaos* **1**, 42–48.

Neishtadt, A. I., Scheeres, D. J., Sidorenko, V. V. and Vasiliev, A. A.: 2002, 'Evolution of comet nucleus rotation', *Icarus* **157**, 205–218.

Peale, S. J. and Lissauer, J. J.: 1989, 'Rotation of Halley's comet' *Icarus* **79**, 396–430.

Samarasinha, N. H. and Belton, M. J. S.: 1995, 'Long-term evolution of rotational states and nongravitational effects for Halley-like cometary nuclei', *Icarus* **116**, 340–358.

Stooke, P. J. and Abergel, A.: 1991 'Morphology of the nucleus of comet P/Halley', *Astron. Astrophys.* **248**, 656–668.

Stooke, P. J. and Abergel, A.: 'Numeric shape model P/Halley nucleus' (unpublished).

Szegö, K., Crifo, J. F., Földy, L., Lagerros, J. S. V. and Rodionov, A. V.: 2001, 'Dynamical effects of comet P/Halley gas production', *Astron. Astrophys*. **370**, L35–L38.

Weeks, C.J.: 1995, 'The effect of comet outgassing and dust emission on the navigation of an orbiting spacecraft', *J. Astronaut. Sci.* **43**, 327–343.

Whipple, F. L.: 1951, 'A comet model. I. Acceleration of comet Encke', *Astrophys. J.* **113**, 464–474.

Wilhelm, K.: 1987, 'Rotation and precession of comet Halley', *Nature* **327**, 27–30.